MEMS Pressure Sensors for Aerospace Applications

Liwei Lin* and Weijie Yun**
*Department of Mechanical Engineering and Applied Mechanics, University of Michigan
2350 Hayward Street, Ann Arbor, MI 48109
TEL: 313-647-6907, FAX: 313-647-3170
lwlin@engin.umich.edu
**SiTek, Inc., Campbell, CA

Abstract: MEMS (Microelectromechanical Systems) pressure sensors have been designed, fabricated and characterized. The fabrication process is fully compatible with IC (Integrated Circuit) fabrication such that multi-functional microelectronics can be directly integrated on the same chip for advanced aerospace applications. These pressure sensors are designed based on the piezoresistive sensing principle on surface micromachined polysilicon thin diaphragms. Both square- and circular-shape diaphragms with thickness of 2 μm and width (diameter) of 100 μm have been designed and fabricated. Prototype pressure sensors with 100 Psi in full scale have a measured sensitivity of 0.15 mV/V/Psi and a maximum linearity error of ±0.1% FSS (Full Scale Span).

1. INTRODUCTION

The spectrum of pressure sensors on a modern aircraft (both military and civil markets) is very broad and complex. Many aircraft systems require pressure sensors as the control elements such as: in engines (oil pressure, compressor pressure, electronic engine control); fuel (pump pressure, fuel regulation); hydraulics (braking system, load control) and environmental applications (air conditioning, pressurization). Future aircraft systems will place increased demands on weight, size, cost, reliability and signal processing of pressure sensors [1]. Micromachined pressure sensors are attractive for aerospace applications because they are aimed for building small size, light weight, low cost and the state of art signal processing electronics units in a single chip. Bulk-micromachined pressure sensors are one of the earliest products made by silicon micromachining [2]. These first generation MEMS pressure sensors were developed in the 1970's. Today, many companies fabricate and sell bulk-micromachined pressure sensors for automobile, industrial and biomedical applications. The measurement range for these pressure sensors can be as high as 10,000 Psi with excellent reliability. For example, Foxboro Company has reported that their pressure sensors can sustain 5 billion 0 to 10,000 Psi pressure cycles. Since these bulk-micromachined pressure sensors have been investigated for many years, the knowledge in both areas of fabrication and design is abundant [3-7].

On the other hand, pressure sensors based on surface micromachined diaphragms were first suggested and fabricated in the 1980s [8]. Thin film deposition and reactive sealing technologies were used to fabricate polysilicon diaphragms with cavities underneath. The back side silicon wet etching process which has been used for bulk-micromachined pressure sensors was avoided [9-12]. These surface micromachined pressure sensors may be more attractive than the bulk-micromachined ones because of the following reasons: first, bulk-micromachined pressure sensors require anisotropic silicon etching [13] to create thin diaphragms from the back side of silicon wafers. This process consumes large areas [14]. For example, if a standard four inch wafer with thickness of 500 μm is used, an area of about 800 x 800 μm^2 is required to make a 100 x 100 μm^2 diaphragm. However, an area of only 100 x 100 μm^2 is needed to make a surface-micromachined diaphragm. Second, bulk-micromachined pressure sensors require post processing including glass to silicon bonding before the final packaging process. Surface micromachined pressure sensors are ready for packaging after the micromachining processes. Finally, surface micromachining is easier to be integrated with IC processes for additional signal processing or device functionality.

This paper presents a new fabrication process for surface micromachined pressure sensors. Design issues for surface micromachined diaphragms are investigated. This new process uses an LPCVD polysilicon deposition step to seal the vacuum cavity [15]. Design optimizations for piezoresistive sensing resistors including position, orientation and length will be addressed.

2. OPERATION PRINCIPLE AND MANUFACTURING METHOD

2.1 Operational Principle

When a uniform pressure is applied to a silicon micro diaphragm, deflection occurs and the internal strain of the diaphragm changes. Silicon is a piezoresistive material [16] such that its resistance changes when the internal strain varies. If the pressure sensing resistors can be constructed and placed on top of the thin diaphragm, pressure can be measured by monitoring the resistance changes. In this paper, a Wheatstone bridge type circuitry has been used to give voltage outputs for pressure measurement. Two sensing resistors are placed inside the diaphragm and the other two referenceresistors are placed outside the diaphragm.

2.2 Small Deflection Theory

In order to determine the optimal design of the sensing resistors including position, orientation and length,

0-7803-4311-5/98/$10.00

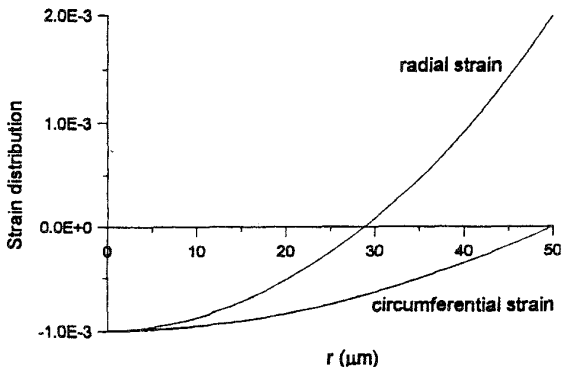

Fig. 1: Radial and circumferential strain distributions of a circular shape diaphragm.

conventional theories of solid mechanics have been investigated. Since linear response is desired, these pressure sensors are designed to be operated in the small deflection region. Two types of diaphragms are considered including both circular and square shapes. They are discussed and analyzed separately.

2.2.1 Circular Plates Under Small Deflection

When a circular plate is under a uniform pressure, q, the governing equation can be derived in terms of the cylindrical coordinate system. The deflection function is derived as [17]:

$$w = \frac{qr^4}{64D} + \frac{C_1 r^2}{4} + C_2 \log\frac{r}{a} + C_3 \tag{1}$$

Where r is radial coordinate in the cylindrical coordinate system; a is the radius; D is the flexural rigidity of the diaphragm; C_1, C_2, C_3 are the constants to be determined by the boundary conditions of the diaphragm. For micro diaphragm with clamped boundary, the radial and circumferential strain can be derived from Eq.(1) as:

$$\varepsilon_r = -\frac{3qa^2(1-\nu^2)}{8Eh^2}\left(1-3\left(\frac{r}{a}\right)^2\right) \tag{2}$$

$$\varepsilon_\theta = -\frac{3qa^2(1-\nu^2)}{8Eh^2}\left(1-\left(\frac{r}{a}\right)^2\right) \tag{3}$$

E is the Young's modulus; ν is Poisson's ratio and h is the thickness of the diaphragm, respectively. Based on these formulas, Figure 1 shows the strain distributions of a circular diaphragm (100 μm in diameter, 2 μm in thickness) which is under a uniform pressure of 100 Psi. Only half of the diaphragm is plotted due to symmetry. It is observed that the radial strain goes from the compressive state (at the center) to the tensile state (at the edge). The circumferential strain is all the way compressive and the maximum value is at the center of the diaphragm. It can be concluded from Fig. 1 that radial strain at the edge of the diaphragm has a higher value than other positions.

2.2.1 Square Plates Under Small Deflection

For square shape plate under small deflection, the analytical solution is more complicated. Timoshenko's method [18] has been used in this paper. A more general case for rectangular shape diaphragms is derived here. It assumes that the deflection of a rectangular shape plate with clamped edges is the summation of three deflection components: w_1, w_2 and w_3. w_1 is the deflection of a simply supported plate under the same uniform pressure; w_2 and w_3 are introduced to preserve the clamped boundary conditions. When a rectangular shape plate with width, a, b and thickness, h, is under a uniform pressure, w_1, w_2 and w_3 can be solved respectively as:

$$w_1 = \frac{4qa^4}{\pi^5 D}\sum_{m=odd}\left(\frac{1}{m^5}\right)(-1)^{\left(\frac{m-1}{2}\right)}\cos\frac{m\pi x}{a}$$
$$\left(1-\left(A_m\tanh A_m+2\right)\left(\frac{\cosh\frac{m\pi y}{a}}{2\cosh A_m}\right)+\frac{\frac{m\pi y}{a}\sinh\frac{m\pi y}{a}}{2\cosh A_m}\right) \tag{4}$$

$$w_2 = \frac{a^2}{2\pi^2 D}\sum_{m=odd}E_m(-1)^{\left(\frac{m-1}{2}\right)}\left(\frac{1}{m^2\cosh A_m}\cos\frac{m\pi x}{a}\right)$$
$$\left(\frac{m\pi y}{a}\sinh\frac{m\pi y}{a}-A_m\tanh A_m\cosh\frac{m\pi y}{a}\right) \tag{5}$$

$$w_3 = \frac{b^2}{2\pi^2 D}\sum_{m=odd}F_m(-1)^{\left(\frac{m-1}{2}\right)}\left(\frac{1}{m^2\cosh B_m}\cos\frac{m\pi x}{b}\right)$$
$$\left(\frac{m\pi x}{b}\sinh\frac{m\pi x}{b}-B_m\tanh B_m\cosh\frac{m\pi x}{b}\right) \tag{6}$$

Where

$$A_m = \frac{m\pi b}{2a}, B_m = \frac{m\pi a}{2b} \tag{7}$$

The values of E_m and F_m can be simulated by the following equations:

$$\frac{4qa^2}{\pi^3 n^4}\left(\frac{A_n}{\cosh^2 A_n}\right)-\tanh A_n = \frac{E_n}{n}\left(\tanh A_n+\frac{A_n}{\cosh^2 A_n}\right)$$
$$+\frac{8na}{\pi b}\sum_{m=odd}F_m\frac{1}{m^3\left(\left(\frac{a}{b}\right)^2+\left(\frac{n}{m}\right)^2\right)^2} \tag{8}$$

$$\frac{4qb^2}{\pi^3 n^4}\left(\frac{B_n}{\cosh^2 B_n}\right)-\tanh B_n = \frac{F_n}{n}\left(\tanh B_n+\frac{B_n}{\cosh^2 B_n}\right)$$
$$+\frac{8nb}{\pi a}\sum_{m=odd}E_m\frac{1}{m^3\left(\left(\frac{a}{b}\right)^2+\left(\frac{n}{m}\right)^2\right)^2} \tag{9}$$

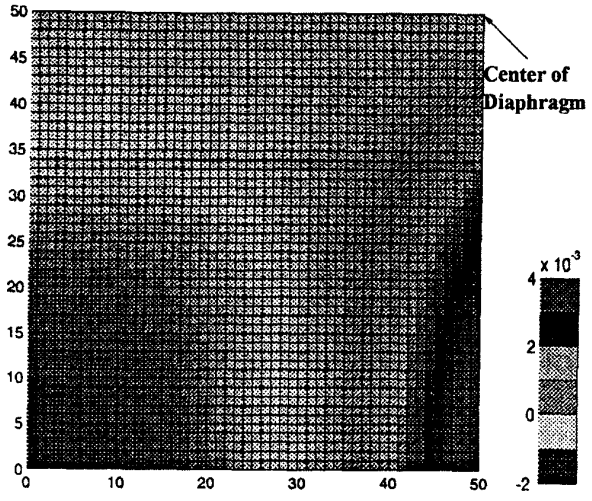

Fig. 2: The x-directional strain distributions on a 100 μm square shape diaphragm (right top quarter) under a pressure of 100 Psi.

The strain distribution can then be derived by using the fundamental stain-displacement relation.

$$\varepsilon_{xx} = -z\frac{\partial^2 w}{\partial x^2}, \varepsilon_{yy} = -z\frac{\partial^2 w}{\partial y^2}, \varepsilon_{xy} = -2z\frac{\partial^2 w}{\partial x \partial y} \quad (10)$$

Figure 2 shows the analytical x-directional strain distributions of a square shape diaphragm (100 μm in length and 2 μm in width) which is under a pressure of 100 Psi. This figure only shows the strain distributions at the right top corner of the diaphragm due to symmetry. The y-directional strain distribution is symmetrical to the x-directional strain with respect to the line of x = y. It is observed that the maximum strain occurs at the middle edge of the square shape diaphragm where the strain is in tensile state. The strain decreases and becomes compressive at the center of the plate.

2.3 Sensitivity of Piezoresistivity

Piezoresistivity of silicon can be analyzed in terms of two directions: parallel or perpendicular direction to the electrical current. The relation can be derived as:

$$\frac{\Delta\rho}{\rho} = F_{par}\varepsilon_l + F_{per}\varepsilon_t \quad (11)$$

The symbol ε_l and ε_t are the strain parallel and perpendicular to the direction of the electrical current, respectively. F_{par} and F_{per} are the gauge factors. They can be represented with respect to the piezoresistive constant Π as:

$$F_{par} = \frac{E(\Pi_l + \nu\Pi_t)}{(1-\nu^2)} \quad (12)$$

$$F_{per} = \frac{E(\Pi_t + \nu\Pi_l)}{(1-\nu^2)} \quad (13)$$

and the changes of resistance can be derived as:

$$\frac{\Delta R}{R} = F_{par}\varepsilon_l + F_{per}\varepsilon_t + \varepsilon_t - \varepsilon_l - \varepsilon_z \quad (14)$$

which can be further derived as:

$$\frac{\Delta R}{R} = \left(F_{par} + \frac{1}{1-\nu}\right)\varepsilon_l + \left(F_{per} + \frac{1-2\nu}{1-\nu}\right)\varepsilon_t \quad (15)$$

The sensitivity of either square or circular shape diaphragms can be calculated according to the above analytical derivation.

2.4 Optimization of Resistor Length

After the sensitivity distribution of the piezoresistive resistor is calculated, the optimal positions for sensing resistors are obtained. The next step is to determine the geometry of the resistor including length and shape for optimal sensitivity. In order to maximize the piezoresistivity effects, line shape resistors are designed for detecting strain changes parallel to the direction of the input current. These line shape resistors are placed at the edges of either the circular or the square shape diaphragm to gain maximum sensitivity as discussed in the previous section. Since misalignments are unavoidable during the fabrication processes, the sensing resistors are designed to have an non-effective portion of 2 μm outside the diaphragm [19]. In order to match the desired impedance and to fully utilize the most sensitive regions on the diaphragms, resistors with several turns are designed in some cases. The turning portions of the resistor will be covered by metal in the manufacturing process such that they are considered as the non-effectiveparts. Only the effectiveparts of the sensor that are inside the diaphragm will be active during pressure measurements. According to the Wheatstone bridge configuration, the output voltage is derived as:

$$V_{out} = \frac{\Delta R_{eff}}{2(R_{eff} + NR) + \Delta R_{eff}} V_{in} \quad (16)$$

where NR is the magnitude of non-effective resistance, R_{eff} is the value of the effective resistance and ΔR_{eff} is the change of the effective resistance due to outside pressure. It can be derived as:

$$\frac{\Delta R_{eff}}{R_{eff}} = \frac{1}{l}\int_L^{L-l}\frac{\Delta R}{R}dx \quad (17)$$

Where l is the length of the effective resistor, is the characteristic length of the diaphragm (radius for a circular

shape diaphragm and half of the width for a square shape diaphragm).

The optimal length of the effective resistor can be calculated by using the above derivation. Figure 3 shows the simulation result for a 100 μm in diameter, 2 μm in thickness, circular shape diaphragm. It is observed that when the effective resistor length is about 12 μm, the diaphragm has an optimal output. Increasing or decreasing this length will reduce the output voltage.

Figure 4 shows the simulation results for square shape diaphragms. The simulation is based on a 100 μm in length, 2 μm in thickness, square shape diaphragm which is under a pressure of 100 Psi. The optimal effective length is about 10 μm in this case. The standard resistor design has one single turn. The sheet resistance is 100 ohm and the width of the resistor is 2 μm. It is observed in Fig. 4 that increasing the number of the turns or the sheet resistance will increase the sensitivity. Increasing the width of the resistor or the thickness of the diaphragm will decrease the sensor output.

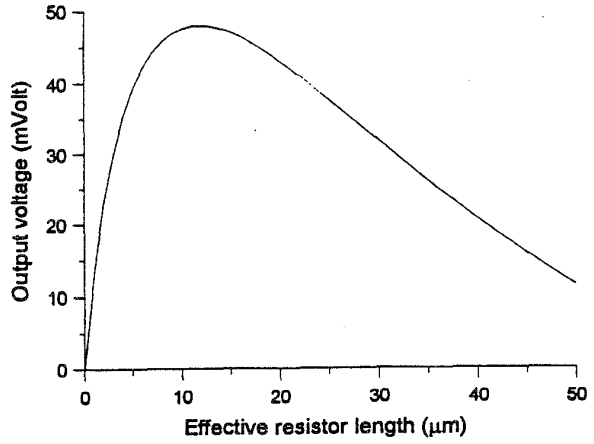

Fig. 3: Optimization analysis of effective resistor length on a circular shape diaphragm.

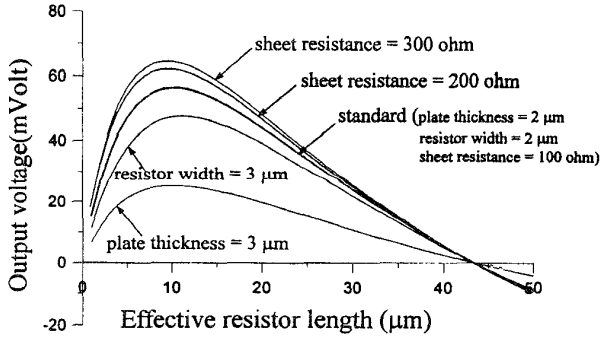

Fig. 4: Optimization analysis of effective resistor length on a square shape diaphragm.

3. FABRICATION PROCESSES AND RESULTS

The fabrication of the sensor requires a total of six masks. There have been many fabrication obstacles to be overcome in the facility we have used in Taiwan. First, the capability of dry etching was not well characterized in the microelectronics lab for our special processes. These processes include the dry etching of thick polysilicon layer and silicon. Therefore, an all wet etching process has been designed and developed to overcome these problems. Second, the LPCVD oxide deposition furnace was not available during our process, a special process involving LPCVD polysilicon deposition and oxidation has been used to replace the LPCVD oxide deposition process.

The process starts with a silicon wafer that is first cleaned. A layer of 0.25 μm LPCVD silicon nitride is deposited and a layer of 0.2 μm thick LPCVD polysilicon is deposited afterwards. The polysilicon layer is the mask for the wet etching process of silicon nitride. The shape of the cavity is defined by using the first mask (mask #1) and polysilicon is etched by using a wet silicon etching solution of HNO_3: H_2O : NH_4F = 64 : 33 : 3 for about one and a half minute. Silicon nitride is then removed by using polysilicon as the masking material in H_3PO_4 liquid at 175°C for about one hour. The cavity area is then formed by the wet silicon etching solution for about 2 minutes. During the same time, the polysilicon layer on top of the silicon nitride is also removed. The depth of the cavity is about 0.5 μm. At the end of the step, a cavity is formed. The wafer is then sent to the thermal oxidation furnace to grow about 1 μm thick silicon dioxide which fully covers the cavity to the originally height. After these steps, Figure 5(a) applies.

A layer of 0.25 μm polysilicon is then deposited and oxidized to form a layer of 0.5 μm thick silicon dioxide. The second mask is then used to define the etch channel shape on the silicon dioxide layer. BufferedHF has been used in this wet etching process for about 5 minutes. A layer of 0.8 μm undoped LPCVD polysilicon is then deposited as the first layer of the diaphragm. The third mask is used to define the etch holes on polysilicon by using wet silicon etchant. Figure 5(b) is the cross sectional view of the process flow at this stage.

The etch hole is in direct contact with the etch channel which is in contact with the cavity. Concentrated HF can etch away the etching channel as well as the cavity which is also made of silicon dioxide. During this etching process, the etch front can be observed under an optical microscope. When the etch front gradually merged and disappeared at the center of the diaphragm, it indicates the completion of the cavity etching. A 1.5 μm thick layer of LPCVD polysilicon is deposited after the cavity etching. This thick polysilicon layer will seal the etch channel since the etch channel is only 0.5 μm in thickness. The sealing process is carried out at an low vacuum environment (LPCVD deposition) such that the cavity is at low vacuum

condition at the end of the sealing process. Figure 5(c) is the process flow diagram up to this step.

After the cavity is sealed and the polysilicon diaphragm is formed, a layer of 0.1 μm thick nitride is deposited. A layer of 0.1 μm thick polysilicon is deposited and then thermal oxidized to form a silicon dioxide layer. Both the silicon dioxide and silicon nitride layers function as the masking layers for the definition of the piezoresistive sensing resistors. The forth mask is used to define the piezoresistive sensors. First, wet etching of the silicon dioxide in bufferedHF is conducted to define the shape of the piezoresistive resistors. The nitride masking layer is then etched by H_3PO_4 liquid at 175°C for about an hour. The shape of the polysilicon resistors is now defined and the wafer is put into the phosphorous pre-deposition furnace for the phosphorus drive-in process for about an hour. This process will grow about 0.1 μm thick thermal oxide which is used as the passivation layer for the device.

The fifth mask is now used to define the contact holes by wet etching the oxide layer. Finally, a layer of aluminum is deposited onto the wafer and the sixth mask is used to define the interconnection lines and contact pads. Wet etching of aluminum is performed by using a solution of H_3PO_4 : HNO_3 : CH_3COOH : H_2O = 50 : 2 : 10 : 9 at 60°C for about 25 seconds. Figure 5(d) shows the completion of these steps. Figure 6 shows top view of a completed surface micromachined pressure sensor with a square shape diaphragm.

Circular shape pressure sensors have also been made by using the same process. Figure 7 is an SEM microphoto of a fabricated circular shape pressure sensor. It has been cleaved such that the cavity underneath the diaphragm can be clearly observed. Metal lines, contact pads, piezoresistive resistors, etch holes and etch channels can also be seen in Figure 7.

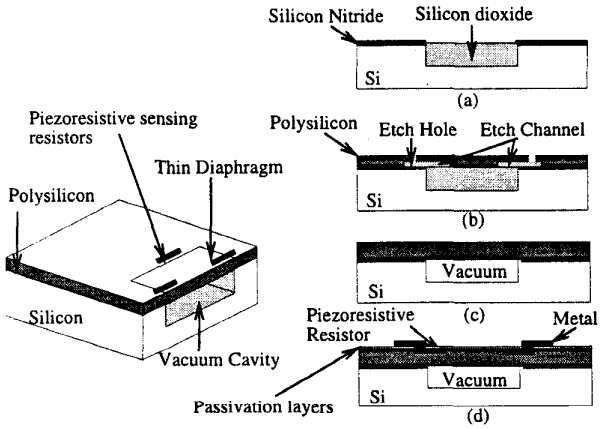

Fig. 5: Process sequence for the surface micromachined pressure sensors.

We have measured the performance of devices made of thin polysilicon diaphragms with the same geometry as shown in Figure 8 [19]. These MEMS pressure sensors have measured sensitivity of 0.15 mV/V/Psi and a maximum linearity error of ±0.1% FSS (Full Scale Span) at room temperature. The sensitivity increases as the temperature decreases because the piezoresistivity changes with temperature [21]. However, the linearity remains excellent at different temperatures as shown in Fig. 8. The temperature range of -40°C to 120°C fit well for the aerospace applications (-60°C is the desired range). These pressure sensors have also demonstrated good performance in long term drift, repeatability, pressure hysteresis and temperature hysteresis. We are still in the process of testing these pressure sensors for qualifications of aerospace standards.

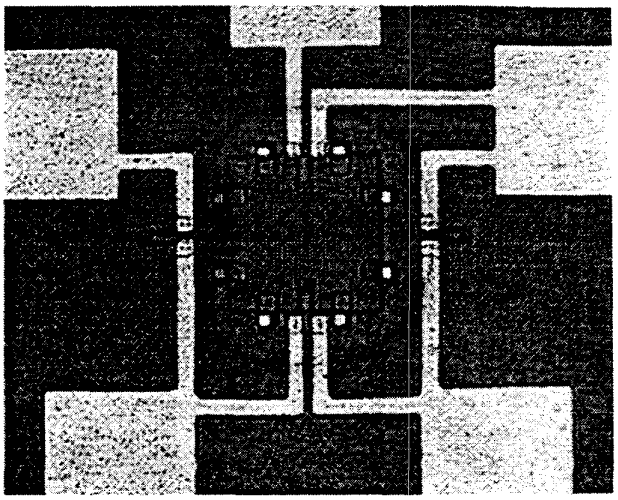

Fig. 6: A fabricated surface micromachined pressure sensor with a square shape diaphragm under an optical microscope.

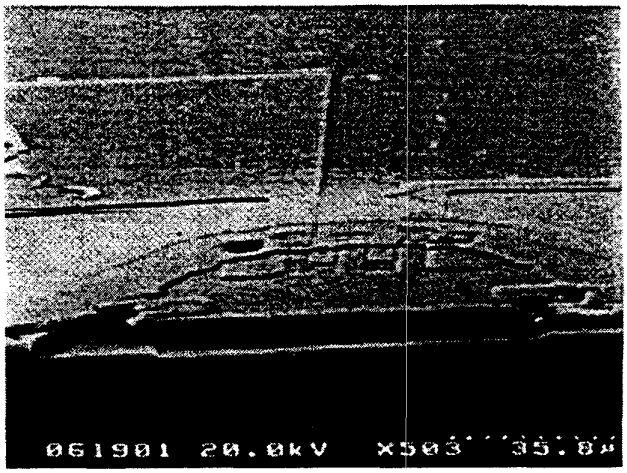

Fig. 7: SEM micrograph showing a cleaved circular micro shell. The cavity underneath the diaphragm can be seen clearly.

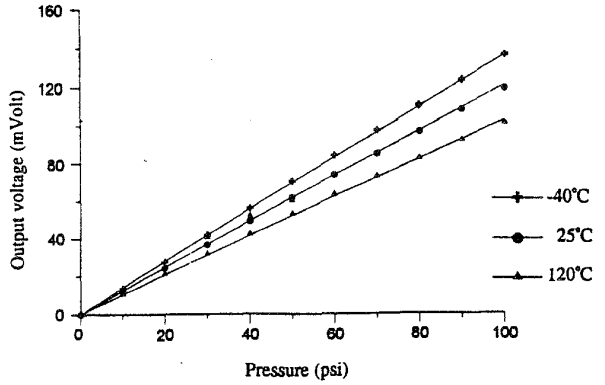

Fig. 8: Testing results of MEMS pressure sensors at different temperatures.

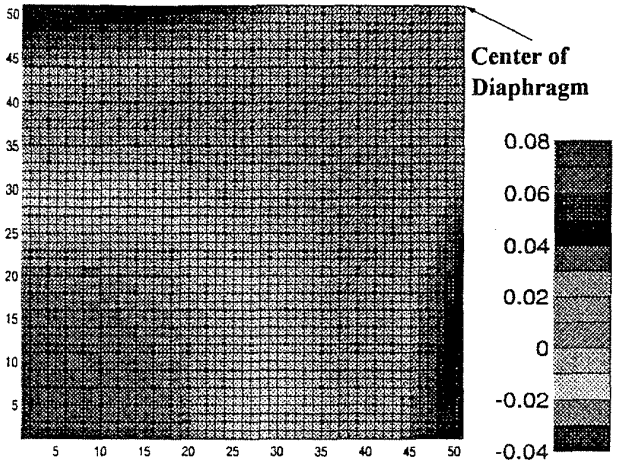

Fig. 8: Sensitivity distributions of a resistor placed 45 degrees off the x axis on a square diaphragm.

4. DISCUSSIONS

Several designs and fabrication issues are discussed for surface micromachined pressure sensors. As discussed in the design principles for pressure sensors, the piezoresistive sensing resistors should be placed at the most sensitive places on the diaphragm. In the pressure sensor design by Motorola, X-ducers [20], where resistors are placed 45 degrees off the axial direction on a square shape diaphragm. To determine the effects of orientation on the placement of these resistors, a sensitivity check for different orientations has been investigated. In a square shape diaphragm, if the resistor is placed with an angle, ϕ, with respect to the x-axial direction, the strains can be derived as:

$$\varepsilon_l = \varepsilon_x \cos^2\phi + 2\varepsilon_{xy}\cos\phi\sin\phi + \varepsilon_y \sin^2\phi \quad (18)$$

$$\varepsilon_t = \varepsilon_x \sin^2\phi - 2\varepsilon_{xy}\cos\phi\sin\phi + \varepsilon_y \cos^2\phi \quad (19)$$

The sensitivities for different orientations of resistor placement can then be calculated. Figure 8 shows the simulation result of the resistance sensitivity diagram for a resistor placed in a direction 45 degrees off the x axis. The sensitivity distribution is, as expected, symmetrical to the line of x = y. The overall sensitivity is comparable to the orientation that is parallel to the x axis as previously discussed but the most sensitive area seems to be decreased.

Other than the orientation, issues including the size and electrical properties of the resistors should also be considered. Some of these parameters have been investigated as shown in Fig. 4. Increasing the turns and sheet resistance are two ways to increase the sensor output. On the other hand, increasing the width of the sensing resistor will reduce the overall output. The depth of the resistor also affects the performance. The top and bottom surfaces have the largest strain changes and the central plane of the diaphragm has zero strain changes according to classical theories of mechanics. It is recommended that the piezoresistive resistors should be constructed close to the surface of the diaphragm. In other words, the drive-in diffusion procedure should be as shallow as possible. Gauge factors of the piezoresistivity are determined by the property of the thin films which can be vary from different process runs. These factors should be characterized and tuned to the optimal values before the pressure sensors are made. Finally, the process developed here has minimized the residual stress by using several annealing processes. However, it is expected that tiny residual stress may exist and the effect of residual stress to the overall performance of the pressure sensors is still under investigation.

The fabrication process developed in this paper has been designed to overcome some process obstacles. A similar process can be developed if dry etching capabilities are well characterized and LPCVD furnaces including silicon dioxide and low stress silicon nitride are available [19]. Ion implantation for defining piezoresistive resistors is also recommended for future development. In that case, photoresist should be used during the ion implantation and the passivation layer should be deposited afterwards.

5. CONCLUSIONS

Design, modeling and fabrication of surface micromachined pressure sensors have been successfully established. The orientation, position and length of the sensing resistors have been fully analyzed. Several specific conclusions can be drawn for the sensor geometries discussed in this paper. For circular shape diaphragms, the most sensitive positions are found to be at the edge of the diaphragm. The sensing resistors should be placed in the radial directions and the optimal length is 12 μm. For square shape diaphragm, the most sensitive locations are at the middle edge of the diaphragm. The sensing resistors should be oriented toward the center and the optimal length is 10 μm. These optimal designs have been analyzed based on conventional solid mechanics theories of shell and plate. Instead of using numerical analysis, analytical solutions are derived. These analytical solutions provide important design guidelines when the dimensions, shapes or orientations of the

diaphragm or sensing resistors are changed. An all wet etching process has been developed to fabricate the surface micromachined pressure sensors. These steps include wet etching of silicon dioxide, silicon nitride, silicon; thin film deposition of nitride, polysilicon; oxidation and drive-in processes. All of these process parameters have been successfully established. These parameters are suitable not only for fabricating the surface micromachined pressure sensors but also for fabricating other MEMS devices.

ACKNOWLEDGMENTS

These devices are fabricated at the at the Semi-Conductor Research Center, National Chiao Tung University, Hsin-Chu, Taiwan with the help of Mr. H.C. Chu. Testing results are conducted at BEI Sensors & Systems Co. LA, USA. The authors would like to thank Dr. L. Wan, Dr. A.M. Madni and their staff, especially, Mr. Tariq Haniff, for technical support.

REFERENCES

[1] S.J. Prosser, "Advances in Sensors for Aerospace Applications," *Sensors and Actuators*, Vol. A37-38, 128-134, 1993.

[2] K.E. Peterson, "Silicon as a Mechanical Material," *Proceedings of the IEEE*, Vol. 70, No. 5, 420-457, 1982.

[3] O.N. Tufte, P.W. Chapman and D. Long, "Silicon Diffused-element Piezoresistive Diaphragm," *J. Appl. Phys.*, pp. 3322, 1962.

[4] S.K. Clark and K.D. Wise, "Pressure Sensitivity in Anisotropically Etched Thin-Diaphragm Pressure Sensors," *IEEE Trans. Electron Devices*, Vol. ED-26, 1887-1896, 1979.

[5] W.H. Ko, "Solid-State Capacitive Pressure Transducers," *Sensors and Actuators*, Vol. 10, 303-320, 1986.

[6] H.L. Char and K.D. Wise, "Scaling Limits in Batch-Fabricated Silicon Pressure Sensors," *IEEE Trans. Electron Devices*, Vol. ED-34, 850-858, 1987.

[7] K. Suzuki, S. Suwazono and T. Ishihara, "CMOS Integrated Silicon Pressure Sensor," *IEEE Journal of Solid-State Circuits*, Vol. 22, 151-156, 1987.

[8] H. Guckel and David Burns, Planar Processed Polysilicon Sealed Cavities for Pressure Transducers Array, *IEDM*,.223-225, 1984.

[9] S. Sugiyama, K. Shimaoka and O. Tabata, "Surface Micromachined Micro-Diaphragm Pressure Sensors," *Proc. of the 6th Int. Conf. on Solid-State Sensors and Actuators, Transducers'91*, 188-191, 1991.

[10] Kung J.T. and H.-S. Lee, "An Integrated Air-Gap-Capacitor Pressure Sensor and Digital Readout with Sub-100 Attofarad Resolution," *Journal. of Microelectromechanical Systems*, Vol. 1, 121-129, 1992.

[11] M.E. Habibi, E. Lueder, T. Kallfass and D. Horst, "A Surface Micromachined Capacitive Absolute Pressure Sensor Array on a Glass Substrate," *Sensors and Actuators*, Vol. A46, 125-128, 1995.

[12] C.H. Mastrangelo, X. Zhang and W.C. Tang, "Surface-micromachined Capacitive Differential Pressure Sensor with Lithographyically Defined Silicon Diaphragm," *J. of Microelectromechanical Systems*, Vol. 5, 89-105, 1996.

[13] E. Bassous, "Fabrication of Novel Three-Dimensional Microstructures by Anisotropic Etching of (100) and (110) Silicon," *IEEE Trans. on Electron Devices*, Vol. ED25, 1178-1185, 1978.

[14] S. Suwazono, H. Tanigawa and M. Hirata, "Diaphragm Thickness Control in Silicon Pressure Sensors Using an Anodic Oxidation Etch-Stop," *J. of the Electrochemical Society*, Vol. 134, 2037-2041, 1987.

[15] Liwei Lin, K.M. McNair, R.T. Howe and A.P. Pisano, "Vacuum Encapsulated Lateral Microresonators," *Proc. of the 7th Int. Conf. on Solid-State Sensors and Actuators, Transducers'93*, 270-273, 1993.

[16] C.S. Smith, "Piezoresistive Effect in Germainium and Silicon," *Phys. Rev.*, Vol. 94, No.1, 42-49, 1954.

[17] W.C. Chien, "Elasticity," (in Chinese), *Asia-East Book Company*, Taipei Taiwan, 1991.

[18] S.P. Timoshenko and S. Woinowsky-Krieger, "Theory of Plates and Shells", 2nd. ed., *McGraw-Hill*, New York, 1959.

[19] Liwei Lin, W. Yun, H.-Chi Chu and M. Chiao, "Surface Micromachined Diaphragm Pressure Sensors with Optimized Piezoresistive Sensing Resistors", *1995 IEEE TENCON*, Hong Kong, 24-27, 1995.

[20] Motorola, "Pressure Sensors - Device Data", Motorola Semiconductor Products Sector, Phonex, Arizona, 1994.

[21] H.-C. Chu, "Surface Micromachined Piezoresistive Pressure Sensors", MS thesis, Institute of Applied Mechanics, National Taiwan University, Taipei, Taiwan, 1996.

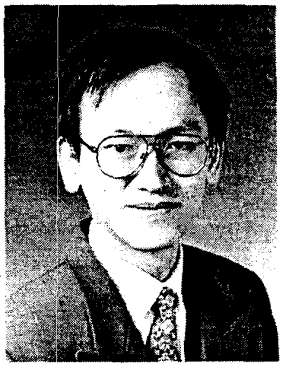

Liwei Lin *is an assistant Professor at the department of Mechanical Engineering and Applied Mechanics, the University of Michigan. He has received the MS and Ph.D. degree in Mechanical Engineering from University of California, Berkeley in 1991 and 1993, respectively. He was a research assistant at Berkeley Sensors and Actuators Center from 1989 to 1993. He joined BEI Electronics Inc. USA from 1993 to 1994 for research and development in microsensors. From 1994 to 1996, he was an associate Professor at the Institute of Applied Mechanics, National Taiwan University, Taiwan. His research interests are in microelectromechanical systems (MEMS) including design, modeling and fabrication of microsensors and microactuators.*

Weijie Yun *is the director at SiTek Inc., a subsidiary of BEI Technologies. He is responsible for establishing SiTek as a leading company in developing and manufacturing micromachining based products. He as held various positions in engineering and management since he joined the company in 1992. He received his M.S. and Ph.D. degrees in Electrical Engineering and Computer Science from University of California, Berkeley.*